Supporting Information

Visible-light-driven prompt and quantitative production of lactic acid from biomass sugars over a N-TiO_2 photothermal catalyst

Yingying Cao,[a] Dandan Chen,[a] Ye Meng,[a] Shunmugavel Saravanamurugan,[b] Hu Li [a,*]

[a] *State Key Laboratory Breeding Base of Green Pesticide & Agricultural Bioengineering, Key Laboratory of Green Pesticide & Agricultural Bioengineering, Ministry of Education, State-Local Joint Laboratory for Comprehensive Utilization of Biomass, Center for R&D of Fine Chemicals, Guizhou University, Guiyang, Guizhou 550025, China.*

[b] *Laboratory of Bioproduct Chemistry, Center of Innovative and Applied Bioprocessing, Sector-81 (Knowledge city), Mohali, India.*

Experimental details

Catalyst characterization

The sample crystal structures and phase compositions were performed using powder X-ray diffraction (XRD, Rigaku Ulitma IV) fitted with an optical source Cu Kα radiation (λ = 1.54178 Å) in the 2θ angle range of 5°-90° at 36 kV and 20 mA. To observe the external morphology and microstructure of the photocatalysts, scanning electron microscope (SEM, JSM-7800F) and transmission electron microscope (TEM, JEM-2800F) were operated at the acceleration voltage of 15 kV and 200 kV, respectively. The elemental composition and chemical state of the samples were analyzed by X-ray photoelectron spectrometer (XPS, Thermo Scientific ESCALAB 250Xi) with Al anode target X-ray source. The XPS test was run under a voltage of 16 kV and a current of 15 mA. Ultraviolet photoelectron spectroscopy (UPS) was carried out using He lamp as a light source (Thermo Scientific ESCALab 250Xi). The specific surface areas and pore size distribution of the samples were carried out by Brunauer-Emmett-Teller (BET, TriStar II 3020). The materials were degassed and adsorbed at 200 °C and -196 °C, respectively. The thickness and width of the samples were evaluated by employing atomic force microscope (AFM, Bruker Dimension Icon). The suspension was dispersed in ethanol and then dropped on the mica sheet. The sample surface morphology was determined based on scanasyst pattern analyst pattern in tapping mode. The recombination rate of photogenerated electrons and holes was explored by photoluminescence (PL, Edinburgh FLS1000) with an excitation light resource of 270 nm at room temperature. The ultraviolet-visible diffuse reflectance spectrum (UV-Vis DRS) measurements were conducted using PERKIN-ELMER Lambda 950 with $BaSO_4$ as a reference object in the detection range of 200-800 nm. The catalyst functional groups were determined by KBr compression using Nicolet 360 FT-IR (Fourier-transform infrared) apparatus. Electro spin-resonance (ESR) spectra of all samples were detected by a Bruker A300 spectrometer.

Electrochemical measurements

The photoelectric performance was tested by electrochemical impedance spectroscopy (EIS) at the electrochemical workstation CHI760E. The conventional standard three-electrode system was utilized.[S1] The 1 × 1 cm Pt sheet was applied as the counter electrode and the saturated calomel electrode as the reference electrode. The electrolyte was obtained by deoxidizing 0.5 M Na_2SO_4 solution in a high-purity N_2 atmosphere for 1 h. The working electrode was prepared by coating the surface of the conductive glass with the prepared catalysts TiO_2 suspension. Firstly, 5 mg catalyst sample was dispersed in 350 μL isopropanol solution. Secondly, 50 μL 10% Nafion was added to the dispersion as flocculant, followed by ultrasonic treatment for 30 min. Finally, 10 μL of suspension was dropped onto the surface of the glassy carbon electrode. The EIS was conducted in the frequency range of 0.01-10^5 Hz.

Theoretical calculations

The first principles were utilized to exercise spin-polarization density functional theory (DFT) calculations.[S2,S3] The calculation was conducted using Perdew-Burke-Ernzerhof (PBE) formulation in generalized gradient approximation (GGA).[S4] The projected augmented wave (PAW) potentials were selected to explain the ionic cores.[S5,S6] Considering the influence of valence electrons, a plane wave basis set with a kinetic energy truncated cutoff of 450 eV was employed. According to the Gaussian smear method, part of the Kohn-Sham orbitals was permitted to be occupied at a width of 0.05 eV. If the energy change does not exceed 10 eV, it is presumed that the electron energy is self-consistent. When the energy change of no more than 0.03 eV/Å is displayed, it indicates that the geometric optimization holds convergence. The vacuum spacing perpendicular to the structural plane is 15 Å. In the case of using 5 × 5 × 2 Monkhorst-Pack *k*-point sampling, the Brillouin zone integration is carried out for the structure of N-TiO_2 and TiO_2. To optimize the equilibrium lattice constant of TiO_2 unit cell, Brillouin zone sampling was run in a 15 × 15 × 15 Monkhorst-Pack *k*-point grid, which was then used to build the supercell model. The model has *p* (2 × 2 × 1) periodicity in the direction of three-dimensional coordinate axis. Through the

structural optimization process, all atoms can be in a relaxed state. Finally, the formation energies (E_f) were calculated. And the calculation formula is $E_f = E_{N/sub} - E_N - E_{sub}$. In this formula, $E_{N/sub}$, E_N, and E_{sub} represent the total energies of the optimized adsorbate/substrate system, the N atom in the structure, and the substrate, respectively. In the calculation process, the Ti atoms in our systems are treated by using U correction. The correction had been set to 3.68 eV.

Supplementary Figures and Tables

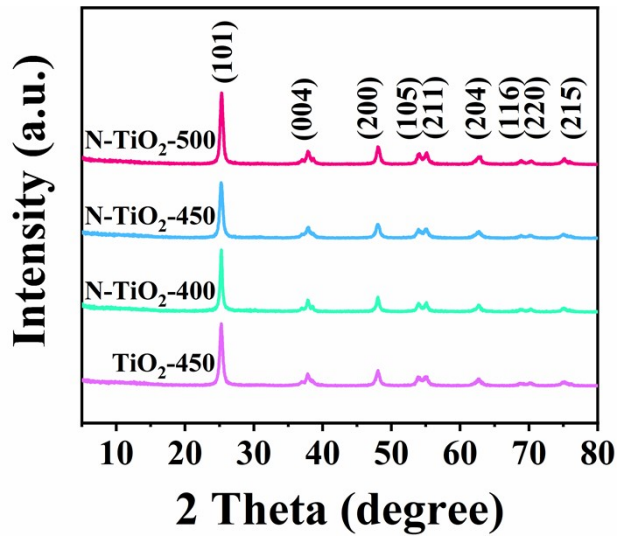

Fig. S1 XRD patterns of N-TiO_2 and pure TiO_2.

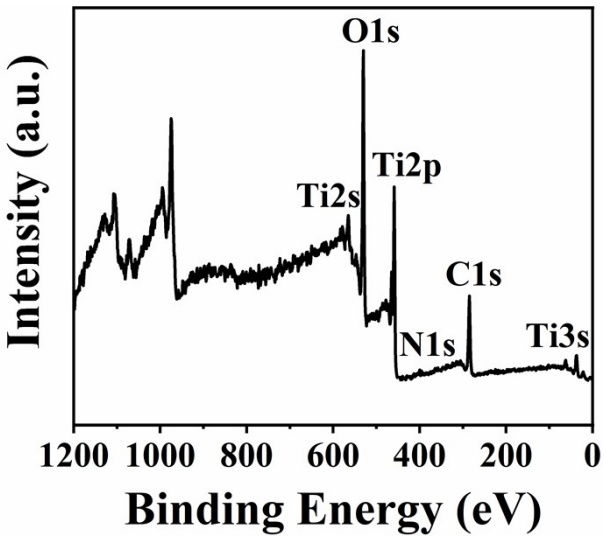

Fig. S2 XPS spectrum of N-TiO_2.

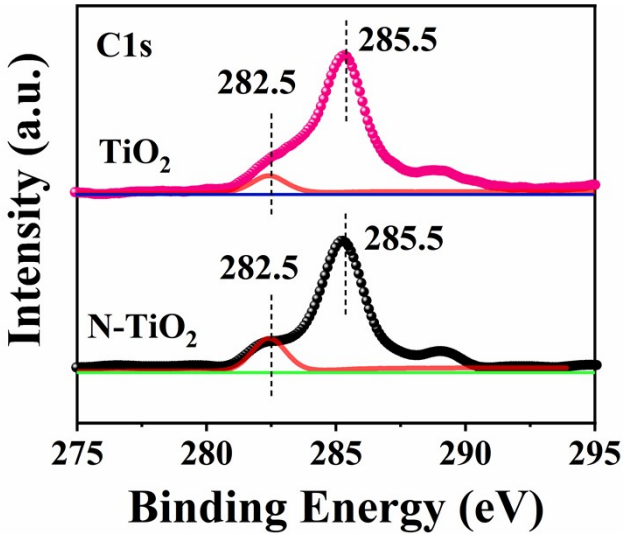

Fig. S3 C1s XPS spectra of TiO_2 and N-TiO_2.

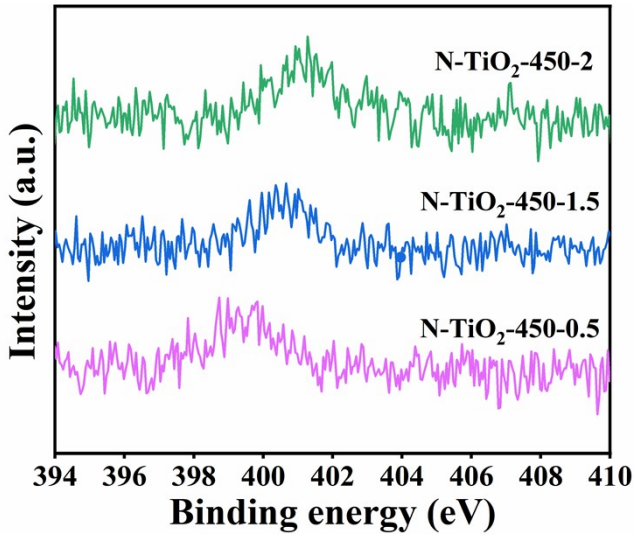

Fig. S4 N 1s XPS spectra of N-TiO_2 in different N contents.

(Urea concentration: 0.5, 1, 1.5, 2 M)

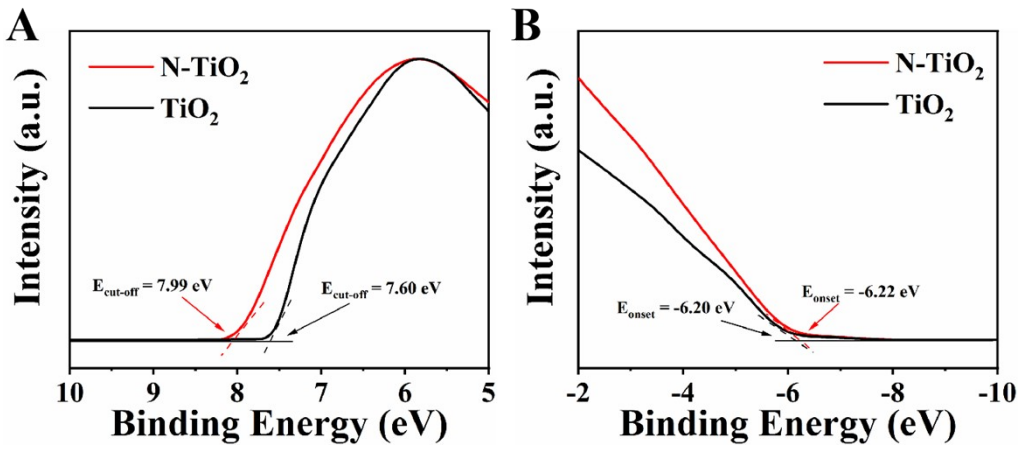

Fig. S5 UPS spectra for different energy edge ranges: (A) cut-off region, and (B) onset region of N-TiO_2 and TiO_2.

The position of the VB can be calculated from the photon energy (hν), the high binding energy cut-off ($E_{cut\text{-}off}$) and the highest occupied molecular orbital (HOMO) energy starting value (E_{onset}) through equations:

$$VB = h\nu\text{-}(E_{cut\text{-}off}\text{-}E_{onset}) \quad \text{(eq. 1)}$$

$$VB\ (N\text{-}TiO_2) = 21.22\text{-}(7.99\text{-}(\text{-}6.22)) = 7.01\ eV \quad \text{(eq. 2)}$$

$$VB\ (TiO_2) = 21.22\text{-}(7.6\text{-}(\text{-}6.2)) = 7.42\ eV \quad \text{(eq. 3)}$$

The positions of the VB of N-TiO_2 and TiO_2 were measured to be -7.01 eV and -7.42 eV vs vacuum level, respectively.

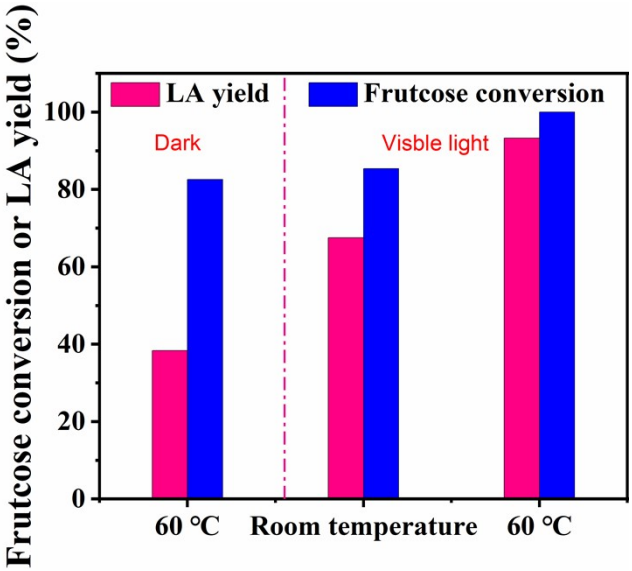

Fig. S6 Effect of different temperatures on the conversion of fructose to lactic acid (LA) under dark and visible light.
(10 mg N-TiO_2, 100 mg fructose, 10 mL 2 M KOH, 1 h)

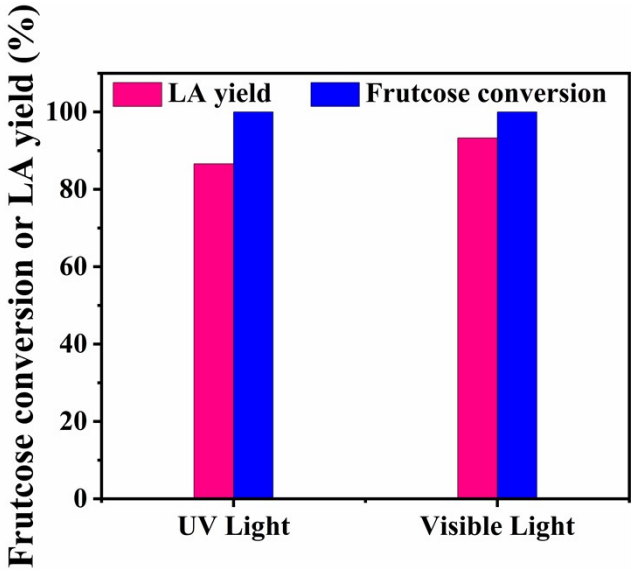

Fig. S7 Effect of different light sources on conversion of fructose to lactic acid (LA) (10 mg N-TiO_2, 100 mg fructose, 10 mL 2 M KOH, 1 h, 60 °C)

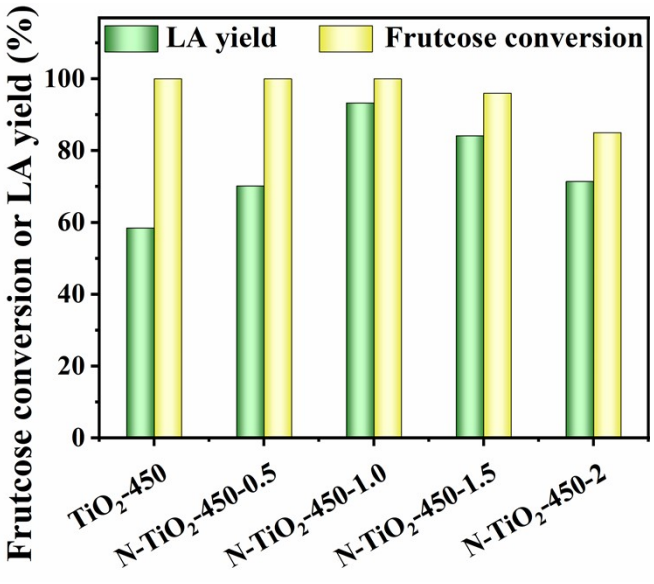

Fig. S8 Effect of different N and C contents on the conversion of fructose to LA (10 mg catalyst, 100 mg fructose, 10 mL 2 M KOH, 1 h visible light, 60 °C, urea concentration: 0.5, 1, 1.5 and 2 M)

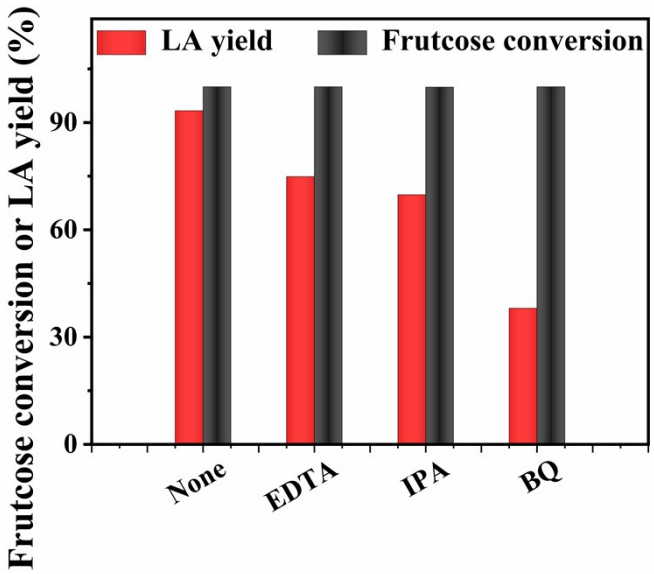

Fig. S9 The effects of different oxidation active species on the synthesis of lactic acid (LA) from fructose
(10 mg N-TiO_2, 100 mg fructose, 10 mL 2 M KOH, 1 h, 60 °C)

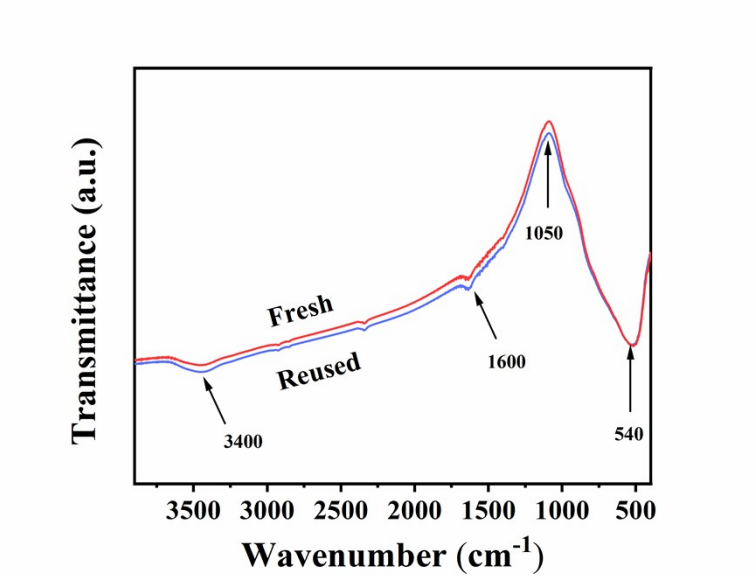

Fig. S10 The FT-IR spectra of fresh and reused N-TiO_2 photothermal catalysts.

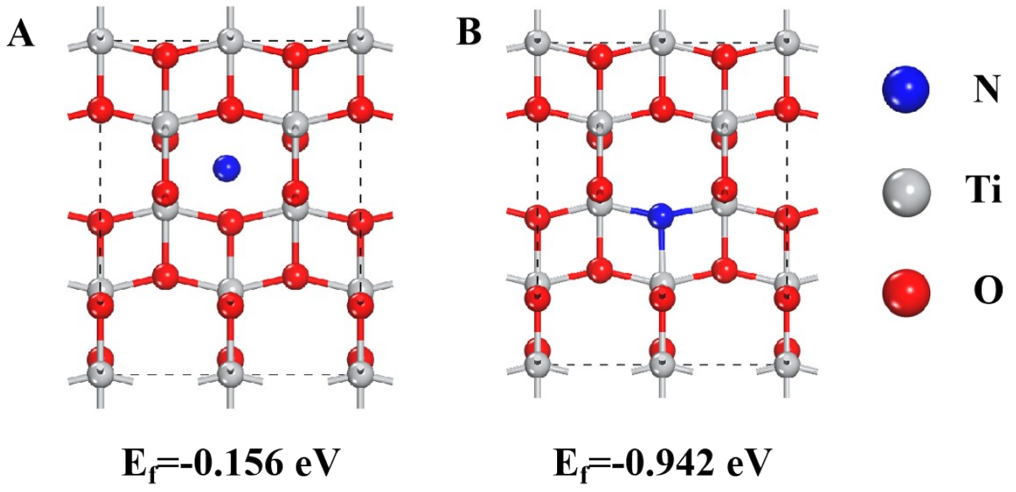

Fig. S11 Structural diagram and formation energies of N-TiO_2 supercell: intermittent N-TiO_2 (A) and replacement N-TiO_2 (B).

Fig. S12 Photocatalytic sugar-to-LA conversion setup.

Table S1. The N and C content of the photothermal catalysts

Entry	Samples	N (at%)	C (at%)
1	TiO_2-450	-	13.71
2	N-TiO_2-450-0.5	2.04	15.24
3	N-TiO_2-450-1	2.45	16.35
4	N-TiO_2-450-1.5	3.52	18.66
5	N-TiO_2-450-2	3.68	20.57

References

[S1] C. Huang, Y. Wen, J. Ma, D. Dong, Y. Shen, S. Liu, H. Ma and Y. Zhang, *Nat. Commun.*, 2021, **12**, 320.

[S2] G. Kresse and J. Furthmüller, *Comput. Mater. Sci*., 1996, **6**, 15-50.

[S3] G. Kresse and J. Furthmüller, *Phys. Rev. B*, 1996, **54**, 11169-11186.

[S4] J. Perdew, K. Burke and M. Ernzerhof, *Phys. Rev. Lett.*, 1997, **77**, 3865-3868.

[S5] G. Kresse and D. Joubert, *Phys. Rev. B*, 1999, **59**, 1758-1775.

[S6] P. E. Blochl, *Phys. Rev. B*, 1994, **50**, 17953-17979.